# TError: towards a better quantification of the uncertainty propagated during the characterization of tephra deposits

S. Biass[1], G. Bagheri[1], W. H. Aeberhard[2], C. Bonadonna[1]

[1]*Section of Earth and Environmental Sciences, University of Geneva, Geneva, Switzerland*
[2]*Research Center for Statistics, University of Geneva, Geneva, Switzerland*

## Abstract

We present *TError*, a *Matlab* package designed to quantify systematically the uncertainty associated with the characterization of tephra deposits, in which the most commonly used methods to quantify eruption source parameters are implemented. Inputs of the code are a range of field-based, model-based and empirical parameters (*i.e.,* clast diameter, crosswind and downwind ranges, thickness measurement, area of isopach contours, bulk deposit density, empirical constants and wind speed), for which the user defines an uncertainty and an associated distribution. The *TError* package contains two main functions. The first function deterministically varies one input parameter at a time and quantifies the sensitivity of each Eruption Source Parameter (ESP; *i.e.,* plume height, erupted volume, mass eruption rate) to the variability of input parameters. The second function propagates input parameters as stochastic distributions of noise through all ESPs. The resulting distributions can then be used to express the uncertainty of physical parameters of explosive eruptions in a systematic way. For both functions, comprehensive reports and sets of figures assist the user in the interpretation of the results. As an example, the *TError* package was applied to Layer 5 of Cotopaxi volcano. Using the median, the $2^{nd}$ percentile and the $98^{th}$ percentile as central value, lower bound and upper bound respectively, a new quantification of the ESP suggests a plume height of $30 \pm 1$ km a.s.l, a mass eruption rate of $1.8^{+0.3}_{-0.2} \times 10^8$ kg s$^{-1}$ and a tephra volume between $0.23^{+0.13}_{-0.04}$ and $0.43^{+0.08}_{-0.06}$ km$^3$, depending on the empirical model used.

## Introduction

Being a direct reflection of plume dynamics, tephra deposits yield a number of features that help characterize key eruptive conditions. Although modern geophysical techniques allow for a rapid quantification of selected eruption source parameters (ESPs) (*e.g.* Prejean & Brodsky, *2011;* Oddsson et al., *2012;* Ripepe et al., *2013)*, the characterization of most historical and all pre-historical eruptions still relies solely on the study of tephra deposits. The identification and the mapping of tephra beds is thus necessary to reconstruct the stratigraphy at a given volcano and to constrain eruptive styles through time, with direct implications for hazard assessment. Typically, a thorough characterization of an explosive eruption includes plume height, wind speed, mass eruption rate (MER), erupted tephra volume/mass, bulk density, eruption duration and total grainsize distribution (TGSD). Since the quantification of such parameters strongly depends on the quality of the exposure (*i.e.* amount of erosion, accessibility, reworking), an inherent uncertainty exists in the interpretation of field deposits, which propagates throughout the characterization of eruptive events. However, the associated uncertainty and the degree of confidence of resulting values are rarely reported in published literature.

Tephra is used here in the generic definition of *Thorarinsson* (1954), describing pyroclastic fragments that are injected into the atmosphere regardless of size, shape or composition. During the last three decades, models have been developed to address the need of the characterization of explosive eruptions, including empirical, statistical and analytical models. These models allow for the characterization of plume height (*Bonadonna & Costa*, 2013; *Burden et al.*, 2011; *Carey & Sparks*, 1986), MER (*Degruyter & Bonadonna*, 2012; *Mastin et al.*, 2009; *Sparks et al.*, 1997; *Sparks*, 1986; *Wilson & Walker*, 1987; *Woodhouse et al.*, 2013) and erupted tephra volume (*Bonadonna & Costa*, 2012; *Bonadonna & Houghton*, 2005; *Burden et al.*, 2013; *Fierstein & Nathenson*, 1992; *Legros*, 2000; *Pyle*, 1989). These methods, with the exception of *Burden et al.* (2013), mostly depend on the compilation of isopleth maps (*i.e.* maps contouring the largest clasts found at given outcrops), and isopach maps (*i.e.* maps contouring the thickness of the deposit).

Three kinds of uncertainties are inherent to the compilation of isopleth and isopach maps. The first kind of uncertainty is related to natural processes. This uncertainty influences how representative the deposit is of the producing eruption. Processes such as reworking and erosion, varying both with latitude and age of the eruption, as well as the accessibility of deposits in different environments, might affect the global picture of the eruptions inferred from various deposits. For example, volume estimates published in the Icelandic literature are traditionally reported as freshly fallen since the work of *Thorarinsson* (1967), where the volume obtained from field measurements is expanded by a factor of 40% to account for compaction processes. Similarly, the fraction of ash ($< 2\,\mathrm{mm}$) can undergo compaction leading to an increase of density and a decrease of thickness up to 50% in a couple of years (*Engwell et al.*, 2013). The second kind of uncertainty relates to measurements. For example, *Biass & Bonadonna* (2011) and *Bonadonna et al.* (2013) show that the measurement of maximum clast and the compilation of isopleth maps is not standardized, considering either 1 or 3 axes of various number (*e.g.,* 1, 3, 5, 10) of clasts and sampling volumes. These different measuring techniques can lead to discrepancies in plume heights between $20 - 40\%$ (*Barberi et al.*, 1995; *Biass & Bonadonna*, 2011). The last kind of uncertainty is related to the subjective choices taken during the contouring of both isopleth and isopach maps. Recently, four volcanologists compiled isopach maps to estimate the volume of the 512 AD eruption of Vesuvius with the 1-segment method of *Fierstein & Nathenson* (1992), resulting in mean discrepancies of 22% for the entire deposit and up to 50% for separate units (*Cioni et al.*, 2011). Similarly, *Klawonn et al.* (2014a) asked 101 volcanologists worldwide to hand contour unpublished thickness measurements from the 1959 Kilauea Iki fallout reported with variable number and geographical distribution of sampling sites. Their work demonstrated *i)* a consistency in volume estimates with different sampling densities, *ii)* a low ( $5 - 8\%$), variability related to the choice of the contour values, and *iii)* a large uncertainty inherent to the construction of the thinnest isopachs, likely to lead to an underestimation of the thinning trend. In order to bypass the subjective choices made during the compilation of isopleth and isopach maps, recent techniques avoid the contouring process either directly inverting mass per

unit area measurements (*Bonasia et al.*, 2010; *Connor & Connor*, 2006; *Klawonn et al.*, 2012; *Volentik et al.*, 2009) or using statistical approaches (*Burden et al.*, 2013).

The variability associated with the various approaches discussed above is rarely reflected in the published literature, where estimates of ESPs are still often provided as single values. For this reason, we developed *TError*, a *Matlab* package designed to help assess the sensitivity of several ESPs to their field-based, model input parameters and to help propagate the uncertainty of these input parameters throughout the characterization of tephra deposits using the most commonly methods present in the literature. The code is designed to assist scientists to forge a critical opinion on the main steps of the characterization of tephra deposits and to interpret resulting values as ranges rather than absolute values. It is written in *Matlab* (tested on version 2009a) and is available on the VHub website. This paper first presents the main aspects of the package, followed by a case study illustrating the package's abilities (Layer 5 of Cotopaxi volcano, Ecuador). An extended review of recent works focused on uncertainty associated with the characterization of tephra deposits and additional applications of the *TError* package is presented by *Bonadonna et al.* (submitted).

## The *TError* package

The *TError* package includes an implementation of one model for the calculation of plume height (*Carey & Sparks*, 1986), three parameterizations for the determination of the MER (*Degruyter & Bonadonna*, 2012; *Mastin et al.*, 2009; *Wilson & Walker*, 1987) and three strategies for the calculation of erupted volume (*Fierstein & Nathenson*, 1992; *Bonadonna & Houghton*, 2005; *Bonadonna & Costa*, 2012). Erupted mass and duration are also quantified. These models were selected for their frequency of use and the variability of assumptions. Ten model input parameters are used, including six field-based parameters (crosswind and downwind ranges of isopleth maps, diameter of the maximum clast, deposit thickness, area of isopach contour and bulk deposit density) as well as four model-dependent parameters (empirical constants of *Wilson & Walker* (1987) and *Mastin et al.* (2009), distal integration limit from *Bonadonna & Houghton* (2005) and wind speed at the tropopause). Note that wind speed can be selected to be either an independent variable (if observed) or propagated from the method of *Carey & Sparks* (1986).

In this paper, we consider the statistical terms *error*, *uncertainty* and *noise* as synonyms, describing the variability around a reference value resulting from measurement error, sampling constraints and operator-dependent decisions. Reference values for all input parameters are supplied by the user and used as the reference value for each ESP. The *relative input uncertainty* (RIU) represents an uncertainty range around each input parameter's reference value and is given in percent, where, for instance, -10% represents a 10% underestimation of the reference value. *Sensitivity analysis* refers to the process of deterministically adding a RIU to one input parameter at a time and assessing its impact on the final ESP. *Error propagation* propagates stochastic distributions of noise around all input parameters to the quantification of all ESPs (*Robert & Casella*, 2004). The *TError* package contains two main code sections. Once relevant input parameters have been estimated, the first code section (`TError_sensitivity.m`) allows the user to visualize the impact of variations of input parameters on the resulting values of ESP. In the second code section (`TError_propagation.m`), the user defines maximum RIU values and distribution types for each input parameter, and the final uncertainty is assessed using Monte Carlo simulations to obtain complete distributions of ESPs. By doing so, features such as asymmetry and heavy tails can be highlighted, whereas derivative techniques generally hide such features. Results are expressed as both raw values, *i.e.,* direct output of the workflow, and as *relative output deviations* (RODs). ROD values are expressed in percent and are quantified as $\dfrac{x - Ref}{Ref \times 100}$, where $x$ and $Ref$ are the raw and the reference value of a given ESP, respectively. Note that ROD values show a spread around 0% and that a negative ROD value implies an underestimation with respect to the reference value. This section describes the selected models and then presents the method used to propagate the uncertainty related to field data.

## Review of the selected models

This section reviews the models coded in *TError* for the quantification of plume height, MER and erupted tephra volume. Here we only describe the relationship used for the calculation of the different ESPs. Since a thorough description and comparison is outside the scope of this paper, the reader is referred to the original publications to forge a global picture of the assumptions behind individual models.

### Plume height

**Carey and Sparks (1986)**   The method of *Carey & Sparks* (1986) relies on the construction of theoretical envelopes within which the vertical velocity of the column and the terminal velocity of a clast of specified size and density are equal. As a result, this method requires the compilation of isopleth maps from which the maximum downwind range is directly related to plume height and wind speed, and from which the crosswind range is related to the plume height only. Note that the wind speed is nil when downwind and crosswind ranges are equal.

The quantification of plume height and wind speed was implemented in *TError* by curve-fitting Figure 16 of *Carey & Sparks* (1986). Figures 16a, 16b, and 16d, were fit using polynomial functions of the $3^{rd}$ degree and Figure 16c was fit using a rational fit of the $5^{th}$ and $3^{rd}$ degrees for the nominator and denominator, respectively. Our implementation includes a linear interpolation between Figures 16a$-$d and can therefore be used for a continuous range of clast diameter and density. The code should nevertheless be used with care when sets of crosswind and downwind ranges result in wind speeds larger than $30\,\mathrm{m\,s^{-1}}$.

### Mass eruption rate

**Wilson and Walker (1987)**   Based on theoretical studies of *Morton et al.* (1956), *Wilson & Walker* (1987) relate the height of a plume to the MER assuming a circular vent and variable exsolved magmatic water weight fraction. The height, $H$, is proportional to the fourth root of the MER ($\mathrm{kg\,s^{-1}}$), where the MER is best fit by (Equation 16 of *Wilson & Walker*, 1987):

$$MER = \left(\frac{H}{k}\right)^4 \tag{1}$$

where $H$ is the maximum plume height (km above the vent) and $k$ is an empirical constant typically set to 0.236 for silicic magmas and between 0.244 and 0.295 for andesitic/basaltic magmas (*Andronico et al.*, 2008; *Scollo et al.*, 2007; *Wehrmann et al.*, 2006).

**Mastin et al. (2009)**   *Mastin et al.* (2009) compiled published data for about 30 well-constrained eruptions in order to empirically identify a best-fit relationship between the plume height and the volumetric flow rate ($\mathrm{m^3\ DRE\ s^{-1}}$). Accounting for a DRE density $\rho_{DRE}$, the mass eruption rate can be estimated as:

$$\dot{V} = \left(\frac{H}{k}\right)^{4.15} \tag{2}$$

where $\dot{V}$ is the DRE volumetric flow rate ($\mathrm{m^3\,s^{-1}}$), $H$ is the plume height (km above the vent) and $k$ is an empirical constant set to 2. In *TError*, $\dot{V}$ is converted to MER ($\mathrm{kg\,s^{-1}}$) by multiplying it by a DRE density of $2500\,\mathrm{kg\,m^{-3}}$ as indicated by *Mastin et al.* (2009). Although there is an uncertainty associated with the DRE density, *TError* only assesses the error of the MER to the uncertainty of the constant $k$.

**Degruyter and Bonadonna 2012**    *Degruyter & Bonadonna* (2012) recently developed a new analytical expression for the calculation of the MER for both vertically-rising and bent-over plumes. This method relates the MER to the plume height and the average wind speed as:

$$MER = \pi \frac{\rho_{a0}}{g'} \left( \frac{\alpha^2 \bar{N}}{10.9} H^4 + \frac{\beta^2 \bar{N}^2 \bar{v}}{6} H^3 \right) \tag{3}$$

where $\rho_{a0}$ is the reference density of the surrounding atmosphere (kg m$^{-3}$), $g'$ the reduced gravity at the source (m s$^{-2}$), $\alpha$ is the radial entrainment coefficient, $\bar{N}$ is the average buoyancy frequency (s$^{-1}$), $H$ is the plume height (m above the vent), $\beta$ is the wind entrainment coefficient and $\bar{v}$ the average wind velocity across the plume height (m s$^{-1}$). If only the wind speed at the tropopause is known, the average wind speed is calculated based on the atmospheric model described in *Bonadonna & Phillips* (2003) where the wind speed linearly decreases from tropopause to ground.

**Tephra volume**    Estimating the volume of tephra fallout is commonly achieved by measuring the thickness of the deposit in strategic locations around the vent in order to infer a thinning trend. The volume can be expressed as a function of the thickness $T$ and the square-root of the area of the isopach $x$ as:

$$V = \int_0^\infty T(x) dA = 2 \int_0^\infty x T(x) dx \tag{4}$$

where $A$ is the area covered by the thickness $T$. Several methods have been proposed during the last decades including the integration of *i)* one or several exponential segments (*Bonadonna & Houghton*, 2005; *Fierstein & Nathenson*, 1992; *Pyle*, 1989), *ii)* a power-law fit (*Bonadonna & Houghton*, 2005), and *iii)* a Weibull fit (*Bonadonna & Costa*, 2012). Here, field measurements are fit using least-square regressions. Little is discussed here regarding the advantages and limitations of the different methods, as extensive reviews can be found in *González-Mellado & Cruz-Reyna* (2010), *Bonadonna & Costa* (2012) and *Daggitt et al.* (2014).

**Fierstein and Nathensen (1992)**    The exponential model states that the thickness $T$ can be expressed as (*Pyle*, 1989):

$$T(x) = T_0 e^{-kA^{0.5}} \tag{5}$$

with $T_0$ being the maximum deposit thickness, $k$ the slope of the exponential segment on plots of $ln(T)$ vs square-root of the isopach area and $A^{0.5}$ the square root of the isopach area. Based on the assumption of ellipsoidal shapes of isopachs *Fierstein & Nathenson* (1992) state that the volume can be estimated as:

$$V = \frac{2T_0}{k^2} \tag{6}$$

with $k$ being the slope of the exponential segment on plots of $ln(T)$ vs square-root of the area. When two exponential segments can be identified, the volume of both segments can be integrated as follows:

$$V = \frac{2T_0}{k^2} + 2T_0 \left[ \frac{k_1 A_{ip}^{0.5} + 1}{k_1^2} - \frac{k A_{ip}^{0.5} + 1}{k^2} \right] e^{-kA_{ip}^{0.5}} \tag{7}$$

where $k$ and $k_1$ are the slopes of the proximal and distal segments respectively and $A_{ip}^{0.5}$ the square-root of the isopach area at the intersect of the two segments. Note that more segments can be added if the right term of Equation 6 is repeated (*e.g.,* Equation 3 of *Bonadonna & Houghton*, 2005).

**Bonadonna and Houghton 2005**    *Bonadonna & Houghton* (2005) state that the thickness $T$ can be described by a power-law relationship, where:

$$T(x) = T_{pl} A^{-0.5m} \qquad (8)$$

with $T_{pl}$ and $m$ being the coefficient and the exponent of the power-law fit. Since $T(x)$ cannot be integrated between 0 and $\infty$, the power-law method requires the choice of proximal (B) and distal (C) integration limits. The volume can then be calculated as:

$$V = \frac{2T_{pl}}{2-m} \left[ C^{(2-m)} - B^{(2-m)} \right] \qquad (9)$$

Typically, the distal limit of integration is the most difficult to identify as the proximal limit can be expressed as:

$$B = \left( \frac{T_0}{T_{pl}} \right)^{\left[ -\frac{1}{m} \right]} \qquad (10)$$

Note that the definition of the distal limit of integration is particularly important for widespread deposits (i.e. with $m < 2$; *Bonadonna & Costa*, 2012).

**Bonadonna and Costa 2012**    *Bonadonna & Costa* (2012) generalized the relation between thickness and isopach area in order to reconcile the advantages of the exponential and power law methods of integration:

$$T(x) = \theta \left[ \frac{\sqrt{A}}{\lambda} \right]^{(n-2)} e^{\left[ \frac{\sqrt{A}}{\lambda} \right]^n} \qquad (11)$$

where $\lambda$ is the decay length scale of the deposit thinning, $\theta$ is a thickness scale and $n$ is a shape parameter. The volume is then defined as:

$$V = \frac{2\theta\lambda^2}{n} \qquad (12)$$

We use here the simplification proposed by *Daggitt et al.* (2014), where $\theta$ is expressed as a function of $\lambda$ and $k$ as:

$$\theta(\lambda, n) = \lambda^{n-2} \sum_{x \in data} \frac{x^{n-2}}{T_{obs}(x)} e^{-\left[ \frac{x}{\lambda} \right]^n} \times \left[ \sum_{x \in data} \left( \frac{x^{n-2}}{T_{obs}(x)} e^{-\left[ \frac{x}{\lambda} \right]^n} \right)^2 \right]^{-1} \qquad (13)$$

Where $x$ is the square root of the isopach area. We also use their suggestion to minimize the following error during the optimization process:

$$Error(\lambda, n) = RSE(\lambda, n) + \ln \left( RSE(\lambda, n) \right) \qquad (14)$$

where the $RSE$ is the relative square error and is defined as:

$$RSE(\lambda, n, \theta) = \sum_{x \in data} \left[ \left( \frac{T_{obs}(x) - T(x)}{T_{obs}(x)} \right)^2 \right] \qquad (15)$$

**Eruption duration**    The eruption duration represents an important parameter in the context of hazard assessment and is quantified as the ratio of mass and MER, where the volume is converted into mass using the bulk deposit density $\rho_{bulk}$:

$$D = \frac{M\rho_{bulk}}{MER} \qquad (16)$$

Here, following *Mastin et al.* (2009), the eruption duration is considered to be the time period over which a significant amount of ash is continuously emitted into the atmosphere.
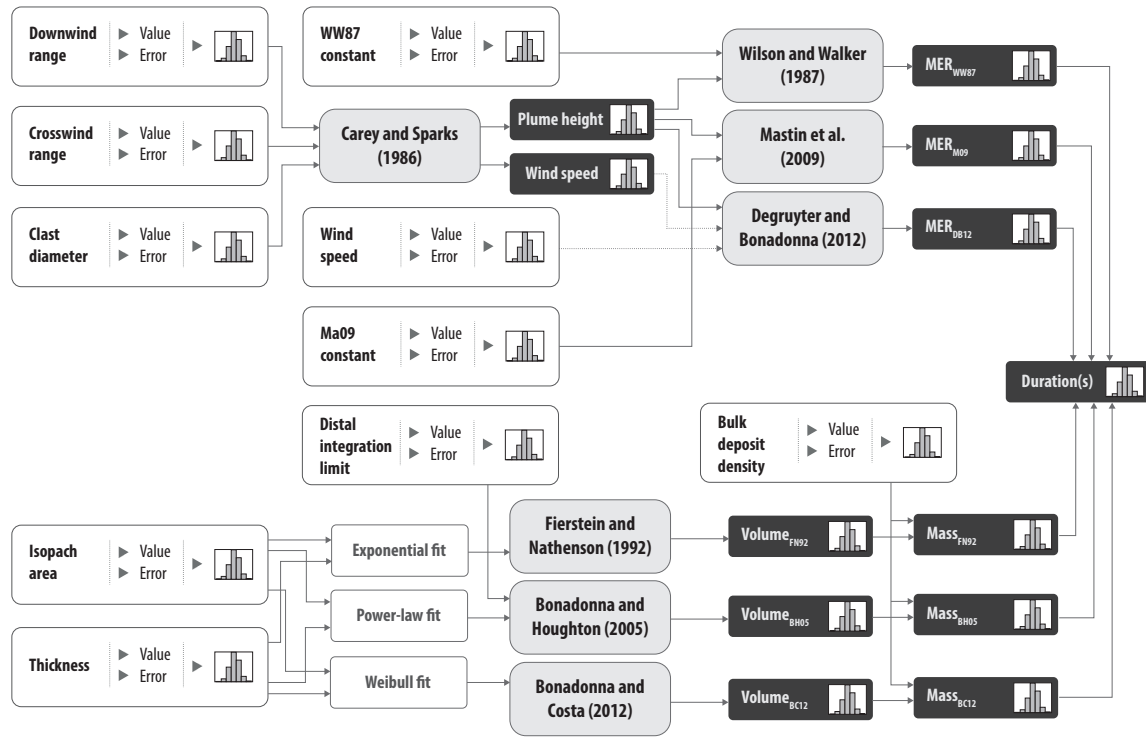
Figure 1: Workflow of the *TError* package.

## Workflow

Figure 1 shows the workflow implemented in *TError*. The crosswind range, downwind range and clast diameter of isopleth contours are used to calculate plume height and wind speed with our implementation of the *Carey & Sparks* (1986) method. The plume height is then converted to MER, deterministically inputting values for the empirical constants of *Wilson & Walker* (1987) and *Mastin et al.* (2009). Since the method of *Degruyter & Bonadonna* (2012) accounts for the effect of the wind on the MER, *TError* either accepts the wind speed as an independent variable or as propagated from the method of *Carey & Sparks* (1986), *i.e.,* directly related to the downwind and crosswind range. In *TError*, the input wind should be the maximum wind speed at the tropopause, interpolated by the code below and above the tropopause according to the atmospheric model of *Bonadonna & Phillips* (2003). The calculation of the tephra volume relies on the compilation of isopach maps, *i.e.,* thickness measurement and area of the isopach contours, including the exponential method with up to three segments defined by the user (*Fierstein & Nathenson*, 1992; *Bonadonna & Houghton*, 2005), the power-law method (*Bonadonna & Houghton*, 2005) and the Weibull method (*Bonadonna & Costa*, 2012). Note that the power-law method requires a distal integration limit. Volumes are converted into mass using a bulk deposit density and combined with MER values to calculate eruption duration.

## Model sensitivity

The first section of the code, *TError_sensitivity*, is designed to allow for the assessment of the sensitivity of each model used to derive ESPs with respect to a variation of input parameters. Once the ten input parameters have been quantified, the code deterministically applies a systematic range of RIU values (typically -40% to 40% at 5% intervals) to each input parameter, independently keeping the error on the remaining input parameters null,

applying the workflow shown in Figure 1 at each increment. Outputs of the *TError_sensitivity* section include *i)* a report where the uncertainty associated with each input parameter is propagated through all ESPs for each RIU increment and *ii)* a set of figures for each ESP summarizing their sensitivity to each input parameter.

### Error propagation

The second section of *TError*, *TError_propagation*, assesses how a distribution of error around each reference input value propagates to each ESP. For each input parameter, the user defines a reference value and RIU which is used to generate an uncertainty distribution from which input values are sampled. Two distributions are available in *TError*, a uniform random distribution, where the RIU serves as maximum and minimum boundaries of the Monte-Carlo simulation, or a Gaussian distribution, where the RIU represents $3\sigma$ (*i.e.,* $\approx 99.7\%$ of the distribution probability mass). In the case of thickness and area of isopach contours, the user assigns a RIU to each thickness/area pair in order to allow for different ranges of uncertainty in distal, medial and proximal areas. The user also inputs the desired number of Monte Carlo simulations.

The workflow is first run using an initial estimate for each input parameter to obtain reference values for each ESP (without uncertainty). For each run of the Monte Carlo simulation, sets of input parameters sampled from the previously defined distributions are propagated through the workflow, resulting in probability distributions for each ESP expressed as raw values and ROD (%) values. Outputs of the *TError_propagation* section include *i)* a report summarizing the uncertainty distributions of all input parameters and ESPs, specifying each reference value, median value and relevant percentiles in raw and ROD forms, and *ii)* figures of probability density functions and boxplots for all input parameters and ESPs.

## Case study

Layer 5 (1180±80 years B.P.) of Cotopaxi volcano, located in Ecuador, is used as a case study to illustrate the package's capabilities.

Table 1: Layer 5, Cotopaxi volcano: parameter ranges[1].

| Parameter | Value |
|---|---|
| Downwind Range | 20.6 km |
| Crosswind Range | 11.3 km |
| Clast Diameter | 1.6 cm |
| Clast Density | 2500 $\mathrm{kg\,m^{-3}}$ |
| DRE Density | 2500 $\mathrm{kg\,m^{-3}}$ |
| Bulk Deposit Density | 1000 $\mathrm{kg\,m^{-3}}$ |
| Distal Integration Limit | 300 km |
| Wind Speed | 19 $\mathrm{m\,s^{-1}}$ |
| Number of Runs | 10,000 |

[1] Refer to *Biass & Bonadonna* (2011)

Layer 5 is a black scoriaceous lapilli fallout with a silica content of 58 wt.% (*Barberi et al.*, 1995). Table 1 and Table 2 summarize the input parameters as characterized by *Biass & Bonadonna* (2011). Isopleth contours were compiled by measuring 3 axes of the 3 largest lithics from a 0.5 m$^2$ area. Thinning trends were best described by two exponential segments with a break in slope located at 9.6 km, a power-law fit and a Weibull fit.

Table 2: Layer 5, Cotopaxi volcano: isopach data[1].

| Thickness (cm) | Area (km$^2$) |
|---|---|
| 100 | 39.4 |
| 50 | 71.3 |
| 30 | 134.4 |
| 20 | 230.3 |
| 15 | 371.1 |
| 10 | 457.8 |

[1] Refer to *Biass & Bonadonna* (2011)

## Sensitivity analysis

Table 3 and Figure 2 show typical outputs from a sensitivity run. Figure 2 is helpful to assess *i)* the dependency of ESPs on their initial inputs, *ii)* the shape of the RODs for both underestimation and overestimation of input parameters, and *iii)* the nature of the relationship between ESPs and input parameters (*e.g.,* positive *vs.* negative, linear *vs.* exponential). Table 3 is a section of tabulated output from a sensitivity run showing only ROD values for ESPs resulting from an application of a RIU of ±10% on the input reference values. The complete tabulated output of a *TError_sensitivity* run is an Excel file with a format identical to Table 3, including as many worksheets as RIU increments. An example can be found in the additional files.

Results for Layer 5 of Cotopaxi volcano show, for instance, slight non-linear relationships between clast diameter and crosswind range with plume height. RIUs of ±10% on the crosswind range, the most important parameter when calculating plume height, result in ROD values of ±5% on the plume height. The MER calculated with the methods of *Wilson & Walker* (1987) and *Mastin et al.* (2009) show strong non-linear negative dependencies on their respective empirical constants. Using *Wilson & Walker* (1987), RIUs of ±10% on the empirical constant, result in ROD values for MER of +52% and −32%, respectively. Similarly, an identical RIU for the constant of *Mastin et al.* (2009) results in ROD values for MER of +55% and −33%, respectively. The method of *Degruyter & Bonadonna* (2012) using the wind speed propagated from *Carey & Sparks* (1986) shows dependencies on clast diameter, crosswind and downwind ranges, where the crosswind range and the clast diameter influence both plume height and wind speed. RIUs of ±10% on clast diameter, crosswind range and downwind range result in symmetrical ROD values for MER of −11%/+15%, −15%/+16% and −13%/+14%, respectively. For the calculation of erupted volume, deposit thickness has a linear, 1:1 positive impact on the final volume for all methods where a thickness increase of 10% results in a tephra volume increased of 10%. Due to the linear nature of the fit, a similar behavior is observed for contour area when using the method of *Fierstein & Nathenson* (1992), where a RIU of ±10% on the area results in ROD values ±10% for the erupted volume. In the particular case of Layer 5 of Cotopaxi, the Weibull fit is close to the exponential fit, and the same trend is observed for the erupted volume calculated with *Bonadonna & Costa* (2012). The uncertainty gradient is lower for the method of *Bonadonna & Houghton* (2005, Power-law), although remaining symmetrical, and a RIU of ±10% on contour area results in ROD values for erupted volume of −9%/ + 8%.

## Error propagation

Figure 3 shows the distributions of sampled input parameters for Layer 5 of Cotopaxi volcano and Figure 4 shows the distributions of selected ESPs resulting from the propagation of noise shown in Figure 3. For all ESP, the median is always close to the reference value (*i.e.,* 0% ROD; Figures 3 and 4, Table 4), and the range between the $25^{th}$-$75^{th}$ and $9^{th}$-$91^{st}$ percentiles represent approximately 1/3 and 2/3 of the spread covered by the

Table 3: Layer 5, Cotopaxi volcano: Typical output of a *Sensitivity* run showing ROD values (in %) of ESPs related to RIUs ±10% around reference values (*i.e.* input values are ±10% smaller and larger than the reference values, respectively). A negative ROD represents an underestimation of the ESP with respect to the initial reference value. References for the calculation methods are listed in the footnote[1] below the table.

| | Downwind Range | Crosswind Range | Clast Diameter | WW87 Constant | Ma09 Constant | Bulk Deposit Density | Thickness | Isopach Contour Area | Distal Integration Limit |
|---|---|---|---|---|---|---|---|---|---|
| **Plume Height** CS86 | — | -5/5 | -2/1 | — | — | — | — | — | — |
| **Wind Speed** CS86 | -25/27 | 20/-17 | -2/5 | — | — | — | — | — | — |
| **MER** WW87 | — | -19/21 | -8/5 | 52/-32 | — | — | — | — | — |
| **MER** MA09 | — | -20/22 | -8/5 | — | 55/-33 | — | — | — | — |
| **MER** DB12 | -13/14 | -15/16 | -11/8 | — | — | — | — | — | — |
| **Volume** FN92 | — | — | — | — | — | — | -10/10 | -10/10 | — |
| **Volume** BH05 | — | — | — | — | — | — | -10/10 | -9/9 | -2/1 |
| **Volume** BC12 | — | — | — | — | — | — | -10/10 | -10/10 | — |
| **Mass** FN92 | — | — | — | — | — | -10/10 | -10/10 | -10/10 | — |
| **Mass** BH05 | — | — | — | — | — | -10/10 | -10/10 | -9/9 | -2/1 |
| **Mass** BC12 | — | — | — | — | — | -10/10 | -10/10 | -10/10 | — |
| **Duration** WW87,FN92 | — | 24/-17 | 9/-4 | -35/46 | — | -10/10 | -10/10 | -10/10 | — |
| **Duration** WW87,BH05 | — | 24/-17 | 9/-4 | -35/46 | — | -10/10 | -10/10 | -9/8 | -2/1 |
| **Duration** WW87,BC12 | — | 24/-17 | 9/-4 | -35/46 | — | -10/10 | -10/10 | -10/10 | — |
| **Duration** MA09,FN92 | — | 25/-18 | 9/-5 | — | -35/49 | -10/10 | -10/10 | -10/10 | — |
| **Duration** MA09,BH05 | — | 25/-18 | 9/-5 | — | -35/49 | -10/10 | -10/10 | -9/8 | -2/1 |
| **Duration** MA09,BC12 | — | 25/-18 | 9/-5 | — | -35/49 | -10/10 | -10/10 | -10/10 | — |
| **Duration** DB12,FN92 | 15/-12 | 17/-14 | 12/-8 | — | — | -10/10 | -10/10 | -10/10 | — |
| **Duration** DB12,BH05 | 15/-12 | 17/-14 | 12/-8 | — | — | -10/10 | -10/10 | -9/8 | -2/3 |
| **Duration** DB12,BC12 | 15/-12 | 17/-14 | 12/-8 | — | — | -10/10 | -10/10 | -10/10 | — |

[1] CS86: *Carey & Sparks* (1986), WW87: *Wilson & Walker* (1987), MA09: *Mastin et al.* (2009), DB12: *Degruyter & Bonadonna* (2012), FN92: *Fierstein & Nathenson* (1992), BH05: *Bonadonna & Houghton* (2005), BC12: *Bonadonna & Costa* (2012)
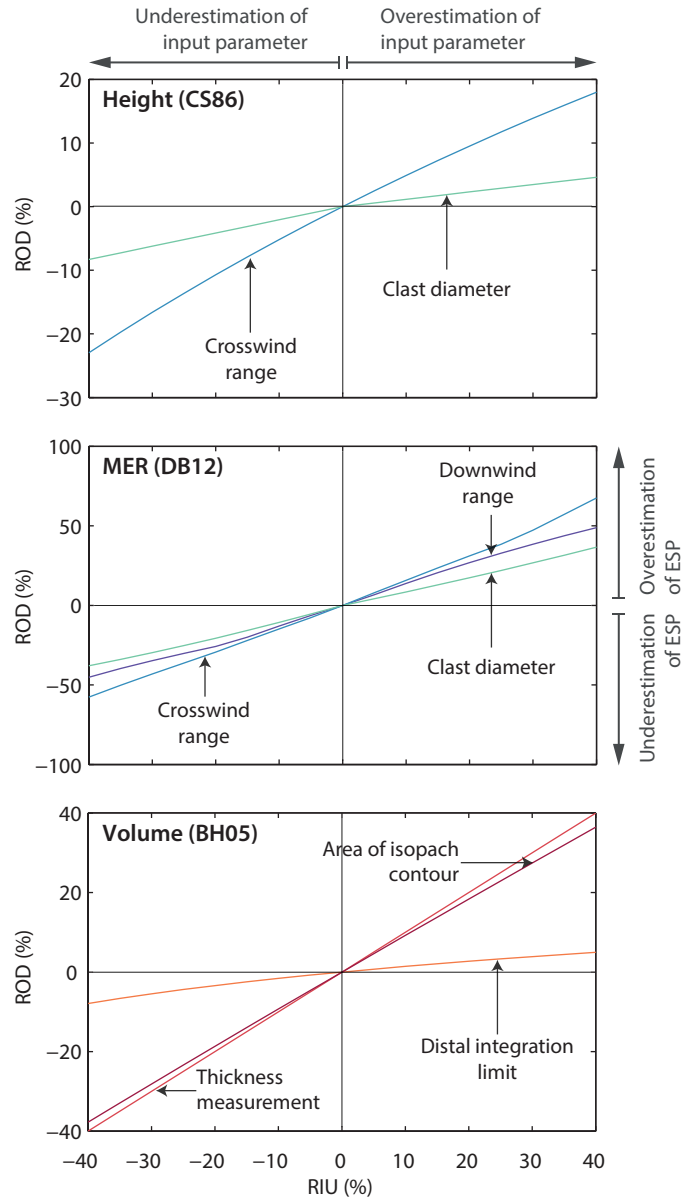
Figure 2: Sensitivity analysis of selected models for Layer 5 of Cotopaxi volcano. Colored lines show the behavior of ESPs with respect to both underestimation and overestimation of the related input parameter compared to the reference value. A RIU of 0% represents an unchanged reference value.
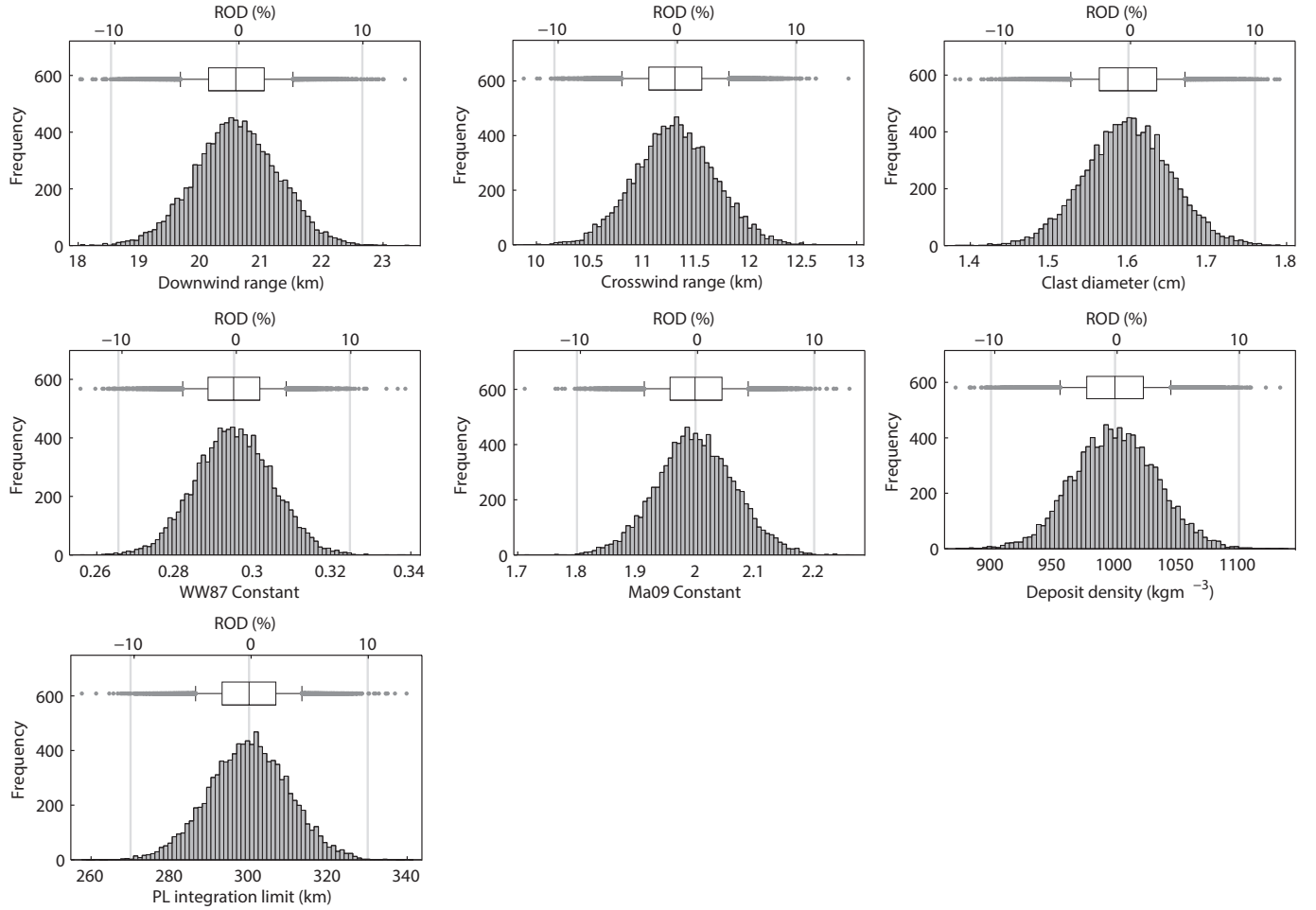
Figure 3: Distributions of input parameters produced by the *TError_propagation* code for Layer 5 of Cotopaxi volcano. The input uncertainty distribution here is Gaussian with $3\sigma$ representing a RIU of 10%. Box and whisker plots represent the $9^{th}$, $25^{th}$, $50^{th}$, $75^{th}$ and $91^{st}$ percentiles and dots represent outliers. The bottom and top x-axis represent the raw values and ROD values, respectively.
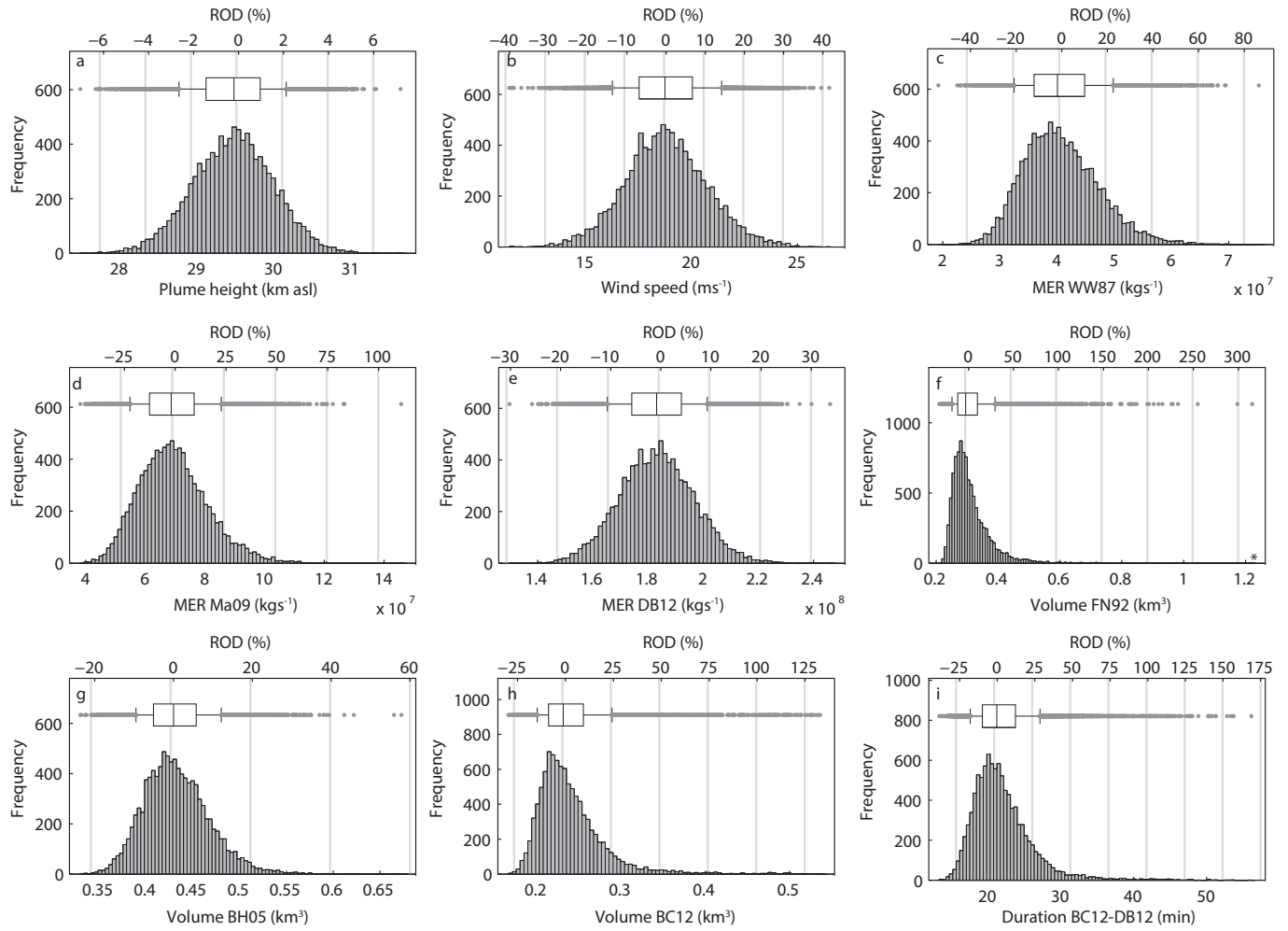
Figure 4: Distributions of selected ESP resulting from propagating the distribution of input parameters shown in Figure 3 for Layer 5 of Cotopaxi volcano. a-b: Plume height and wind speed calculated with the method of *Carey & Sparks* (1986); c-e: MER calculated with the methods of *Wilson & Walker* (1987), *Mastin et al.* (2009) and *Degruyter & Bonadonna* (2012), respectively; f-h: Tephra volumes calculated with the methods of *Fierstein & Nathenson* (1992), *Bonadonna & Houghton* (2005) and (*Bonadonna & Costa*, 2012), respectively; i: duration calculated as the ratio between mass (converted from the volume obtained with the method of *Bonadonna & Costa* (2012)) and MER (*Degruyter & Bonadonna*, 2012).

Table 4: Layer 5, Cotopaxi volcano: Distribution summary for each ESP after a *Propagation* run (Figure 4), showing raw values and ROD values (in %).

| | Units | Ref. Value | Median Value | Min. Value | $25^{th}$ % Value | $75^{th}$ % Value | Max. Value |
|---|---|---|---|---|---|---|---|
| **Plume Height** CS86 | $km$ | 29.5 | 29.5 | 27.5 | 29.1 | 29.8 | 31.6 |
| | | | | -6.7% | -1.2% | 1.2% | 7.3% |
| **Wind Speed** CS86 | $m\,s^{-1}$ | 18.7 | 18.8 | 11.4 | 17.5 | 20.0 | 26.5 |
| | | | | -39.2% | -6.5% | 6.9% | 41.4% |
| **MER** WW87 | $\times 10^7\ kg\,s^{-1}$ | 4.0 | 4.0 | 1.9 | 3.6 | 4.5 | 7.5 |
| | | | | -52.0% | -10.2% | 11.9% | 88.0% |
| **MER** MA09 | $\times 10^7\ kg\,s^{-1}$ | 6.9 | 6.9 | 3.8 | 6.1 | 7.6 | 15.0 |
| | | | | -44.4% | -10.6% | 11.2% | 112.3% |
| **MER** DB12 | $\times 10^7\ kg\,s^{-1}$ | 18.0 | 18.0 | 13.0 | 17.0 | 19.0 | 25.0 |
| | | | | -29.1% | -4.9% | 4.9% | 34.3% |
| **Volume** FN92 | $km^3$ | 0.3 | 0.3 | 0.2 | 0.3 | 0.3 | 2.5 |
| | | | | -28.9% | -8.6% | 12.8% | 738.8% |
| **Volume** BH05 | $km^3$ | 0.4 | 0.4 | 0.3 | 0.4 | 0.5 | 0.7 |
| | | | | -23.2% | -5.0% | 5.6% | 56.7% |
| **Volume** BC12 | $km^3$ | 0.2 | 0.2 | 0.2 | 0.2 | 0.3 | 0.5 |
| | | | | -28.1% | -7.6% | 10.3% | 132.0% |
| **Mass** FN92 | $\times 10^{11}\ kg$ | 2.9 | 3.0 | 2.0 | 2.7 | 3.3 | 24.0 |
| | | | | -32.4% | -8.6% | 13.3% | 706.4% |
| **Mass** BH05 | $\times 10^{11}\ kg$ | 4.3 | 4.3 | 3.3 | 4.1 | 4.6 | 6.8 |
| | | | | -22.6% | -5.4% | 6.0% | 59.1% |
| **Mass** BC12 | $\times 10^{11}\ kg$ | 2.3 | 2.3 | 1.6 | 2.1 | 2.6 | 5.5 |
| | | | | -30.1% | -7.9% | 10.5% | 136.4% |
| **Duration** WW87,FN92 | $min$ | 121.3 | 126.0 | 54.0 | 108.0 | 144.0 | 1086.0 |
| | | | | -55.0% | -13.8% | 17.9% | 770.6% |
| **Duration** WW87,BH05 | $min$ | 176.0 | 180.0 | 84.0 | 156.0 | 204.0 | 402.0 |
| | | | | -52.2% | -11.6% | 13.5% | 124.7% |
| **Duration** WW87,BC12 | $min$ | 95.1 | 96.0 | 48.0 | 84.0 | 114.0 | 288.0 |
| | | | | -50.1% | -13.3% | 15.2% | 192.0% |
| **Duration** MA09,FN92 | $min$ | 71.0 | 72.0 | 36.0 | 60.0 | 84.0 | 822.0 |
| | | | | -53.9% | -13.8% | 18.2% | 1028.6% |
| **Duration** MA09,BH05 | $min$ | 102.9 | 102.0 | 54.0 | 90.0 | 120.0 | 228.0 |
| | | | | -51.1% | -11.6% | 13.9% | 116.0% |
| **Duration** MA09,BC12 | $min$ | 55.6 | 60.0 | 24.0 | 48.0 | 66.0 | 168.0 |
| | | | | -52.8% | -13.2% | 15.9% | 191.4% |
| **Duration** DB12,FN92 | $min$ | 26.6 | 30.0 | 18.0 | 24.0 | 30.0 | 234.0 |
| | | | | -39.6% | -10.0% | 14.6% | 773.9% |
| **Duration** DB12,BH05 | $min$ | 38.6 | 42.0 | 24.0 | 36.0 | 42.0 | 66.0 |
| | | | | -35.2% | -7.1% | 8.2% | 61.9% |
| **Duration** DB12,BC12 | $min$ | 20.9 | 24.0 | 12.0 | 18.0 | 24.0 | 54.0 |
| | | | | -37.2% | -9.4% | 12.0% | 164.3% |

CS86: *Carey & Sparks* (1986), WW87: *Wilson & Walker* (1987), MA09: *Mastin et al.* (2009), DB12: *Degruyter & Bonadonna* (2012), FN92: *Fierstein & Nathenson* (1992), BH05: *Bonadonna & Houghton* (2005), BC12: *Bonadonna & Costa* (2012)

Table 5: Layer 5, Cotopaxi volcano: Median value and percent deviation from reference value for ESPs when using Gaussian (G) and uniform random (U) distributions of input error with a maximum RIU of 10%.

| | Units | Median | | Interpercentile Ranges *(values are % deviation from reference)* | | | | | |
| | | | | 0.25–0.75 | | 0.09–0.91 | | 0.02–0.98 | |
| | | G | U | G | U | G | U | G | U |
|---|---|---|---|---|---|---|---|---|---|
| **Plume height** CS86 | $km$ | 29.5 | 29.4 | 2.4 | 5.1 | 4.7 | 8.5 | 7.2 | 11.1 |
| **Wind speed** CS86 | $ms^{-1}$ | 18.8 | 19.0 | 13.4 | 26.4 | 27.5 | 51.7 | 43.9 | 71.6 |
| **MER** WW87 | $\times 10^7\ kgs^{-1}$ | 4.0 | 4.1 | 22.1 | 41.9 | 43.3 | 80.1 | 67.7 | 110.9 |
| **MER** MA09 | $\times 10^7\ kgs^{-1}$ | 6.9 | 7.1 | 21.8 | 43.5 | 44.5 | 84.0 | 69.3 | 118.5 |
| **MER** DB12 | $\times 10^7\ kgs^{-1}$ | 18.0 | 18.0 | 9.8 | 18.0 | 19.7 | 35.0 | 30.5 | 52.0 |
| **Volume** FN92 | $km^3$ | 3.0 | 3.2 | 21.4 | 26.0 | 47.0 | 60.2 | 90.6 | 116.5 |
| **Volume** BH05 | $km^3$ | 4.3 | 4.3 | 10.6 | 12.7 | 21.3 | 25.0 | 33.7 | 40.0 |
| **Volume** BC12 | $km^3$ | 2.3 | 2.5 | 17.9 | 21.4 | 38.4 | 48.4 | 76.5 | 98.9 |
| **Mass** FN92 | $\times 10^{11}\ kg$ | 3.0 | 3.2 | 21.9 | 26.6 | 48.3 | 63.1 | 92.1 | 120.8 |
| **Mass** BH05 | $\times 10^{11}\ kg$ | 4.3 | 4.3 | 11.4 | 14.9 | 23.1 | 29.9 | 36.6 | 46.3 |
| **Mass** BC12 | $\times 10^{11}\ kg$ | 2.3 | 2.5 | 18.4 | 22.9 | 39.7 | 51.1 | 78.6 | 102.1 |
| **Duration** WW87,FN92 | $min$ | 126 | 138 | 31.7 | 50.2 | 66.1 | 101.2 | 119.9 | 173.8 |
| **Duration** WW87,BH05 | $min$ | 180 | 186 | 25.1 | 43.7 | 49.8 | 84.2 | 76.9 | 122.7 |
| **Duration** WW87,BC12 | $min$ | 96 | 108 | 28.5 | 46.2 | 60.2 | 94.3 | 107.4 | 153.6 |
| **Duration** MA09,FN92 | $min$ | 72 | 78 | 32.0 | 51.5 | 68.2 | 105.4 | 117.0 | 179.3 |
| **Duration** MA09,BH05 | $min$ | 102 | 108 | 25.5 | 45.7 | 50.6 | 87.5 | 79.9 | 128.7 |
| **Duration** MA09,BC12 | $min$ | 60 | 60 | 29.1 | 49.0 | 61.4 | 98.8 | 106.2 | 160.8 |
| **Duration** DB12,FN92 | $min$ | 30 | 30 | 24.6 | 32.6 | 53.0 | 73.4 | 98.1 | 135.5 |
| **Duration** DB12,BH05 | $min$ | 42 | 42 | 15.3 | 23.1 | 31.1 | 46.2 | 48.2 | 72.0 |
| **Duration** DB12,BC12 | $min$ | 24 | 24 | 21.4 | 30.1 | 45.0 | 62.6 | 84.4 | 115.8 |

CS86: *Carey & Sparks* (1986), WW87: *Wilson & Walker* (1987), MA09: *Mastin et al.* (2009), DB12: *Degruyter & Bonadonna* (2012), FN92: *Fierstein & Nathenson* (1992), BH05: *Bonadonna & Houghton* (2005), BC12: *Bonadonna & Costa* (2012)

$2^{nd} - 98^{th}$ percentiles, respectively (Table 5). The plume height shows a symmetric distribution of uncertainty, with minimum and maximum values of $\pm7\%$ of the reference value. The first and third quartiles (Q1 and Q3, the $25^{th}$ and $75^{th}$ percentiles, respectively), are $\pm1.2\%$ of the reference, respectively. The distribution of wind speeds, also symmetrical, carries a larger uncertainty envelope with minimum and maximum values of $-39\%$ and $+41\%$, respectively, and Q1 and Q3 at $\pm7\%$ based on the reference value.
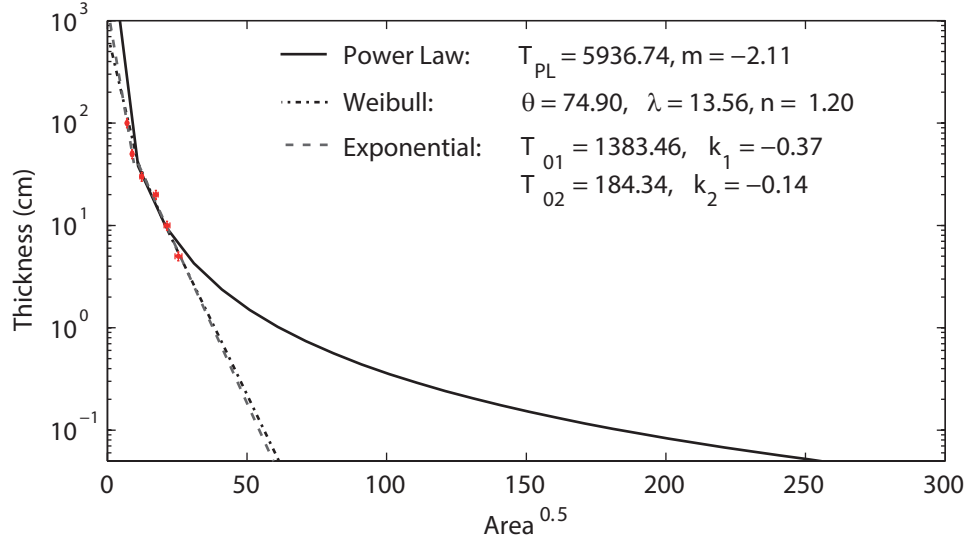


Figure 5: Fits used in volume calculation for Layer 5 of Cotopaxi volcano.

MER estimated with the methods of *Wilson & Walker* (1987) and *Mastin et al.* (2009) introduce an asymmetry in the resulting distributions of RODs due to the exponential nature of their formulations giving rise to lognormal-distributed noise. For instance, MER calculated with the method of *Wilson & Walker* (1987) results in a minimum of $-52\%$, a maximum of $+88\%$, Q1 at $-10\%$, and Q3 at $+12\%$. Similarly, the model of *Mastin et al.* (2009) results in a minimum for the MER of $-44\%$, a maximum of $+112\%$ and Q1 and Q3 at $\pm11\%$. Although not perfectly Gaussian, the distribution of MER resulting from the method of *Degruyter & Bonadonna* (2012) shows a minimum of $-29\%$, a maximum of $+34\%$ and Q1 and Q3 at $\pm5\%$. Figures 5 and 6 show volume fits for the reference values and the variability of fits with uncertainty on deposit thickness and isopach area, respectively. The method of (*Bonadonna & Houghton*, 2005) presents the smallest spreads of volumes with a minimum of $-23\%$, a maximum of $+57\%$, Q1 at $-5\%$ and Q3 at $+6\%$, followed by the method of *Bonadonna & Costa* (2012) with a minimum of $-28\%$, a maximum of $+132\%$, Q1 at $-8\%$ and Q3 at $+10\%$. The method of *Fierstein & Nathenson* (1992) has a similar minimum ($-29\%$), but the maximum goes as high as $+738\%$ due to the variability of the proximal segments defined on two points (Figure 6), with Q1 at $-9\%$ and Q3 at $+13\%$. The distributions of mass follow the same behavior as volume. Combining the distributions of MER and mass, the largest and smallest spreads are given by combining the methods of *Mastin et al.* (2009) and *Fierstein & Nathenson* (1992) with a minimum of $-54\%$, a maximum of $+1027\%$, Q1 at $-14\%$ and Q3 at $+18\%$, and *Degruyter & Bonadonna* (2012) and *Bonadonna & Houghton* (2005) with a minimum of $-35\%$, a maximum of $+62\%$, Q1 at $-7\%$ and Q3 at $+8\%$.

For simplicity, we assume a $\pm10\%$ error on all input parameters and a Gaussian distribution of error, and perform 10,000 Monte Carlo simulations, propagating wind speed from the method of *Carey & Sparks* (1986). Figures 3 and 4 and Table 4 present the results of a *TError_propagation* run for Layer 5 of Cotopaxi volcano. The complete tabulated output, available in the additional files, includes a statistical summary (*i.e.,* selected

Table 6: Layer 5, Cotopaxi volcano: Characterization of ESPs describing 96% of the population, *i.e.*, the 2% − 98% range.

| ESP | Units | Error Ranges |
|---|:---:|---:|
| **Plume Height** CS86 | $km$ | $29.5^{+1.0}_{-1.1}$ |
| **Wind Speed** CS86 | $m\,s^{-1}$ | $18.8^{+4.2}_{-4.0}$ |
| **MER** WW87 | $\times 10^7\ kg\,s^{-1}$ | $4.0^{+1.6}_{-1.1}$ |
| **MER** MA09 | $\times 10^7\ kg\,s^{-1}$ | $6.9^{+2.8}_{-2.0}$ |
| **MER** DB12 | $\times 10^7\ kgs^{-1}$ | $18.0^{+3.0}_{-2.0}$ |
| **Volume** FN92 | $km^3$ | $0.3^{+0.02}_{-0.06}$ |
| **Volume** BH05 | $km^3$ | $0.43^{+0.08}_{-0.06}$ |
| **Volume** BC12 | $km^3$ | $0.23^{+0.13}_{-0.04}$ |
| **Mass** FN92 | $\times 10^{11}\ kg$ | $3.0^{+2.1}_{-0.7}$ |
| **Mass** BH05 | $\times 10^{11}\ kg$ | $4.3^{+2.1}_{-0.7}$ |
| **Mass** BC12 | $\times 10^{11}\ kg$ | $2.3^{+1.4}_{-0.4}$ |
| **Duration** WW87,FN92 | $min$ | $126^{+102}_{-42}$ |
| **Duration** WW87,BH05 | $min$ | $180^{+78}_{-54}$ |
| **Duration** WW87,BC12 | $min$ | $96^{+72}_{-30}$ |
| **Duration** MA09,FN92 | $min$ | $72^{+60}_{-24}$ |
| **Duration** MA09,BH05 | $min$ | $102^{+54}_{-30}$ |
| **Duration** MA09,BC12 | $min$ | $60^{+36}_{-24}$ |
| **Duration** DB12,FN92 | $min$ | $30^{+18}_{-12}$ |
| **Duration** DB12,BH05 | $min$ | $42^{+6}_{-12}$ |
| **Duration** DB12,BC12 | $min$ | $24^{+12}_{-6}$ |

CS86: *Carey & Sparks* (1986), WW87: *Wilson & Walker* (1987), MA09: *Mastin et al.* (2009), DB12: *Degruyter & Bonadonna* (2012), FN92: *Fierstein & Nathenson* (1992), BH05: *Bonadonna & Houghton* (2005), BC12: (*Bonadonna & Costa*, 2012)
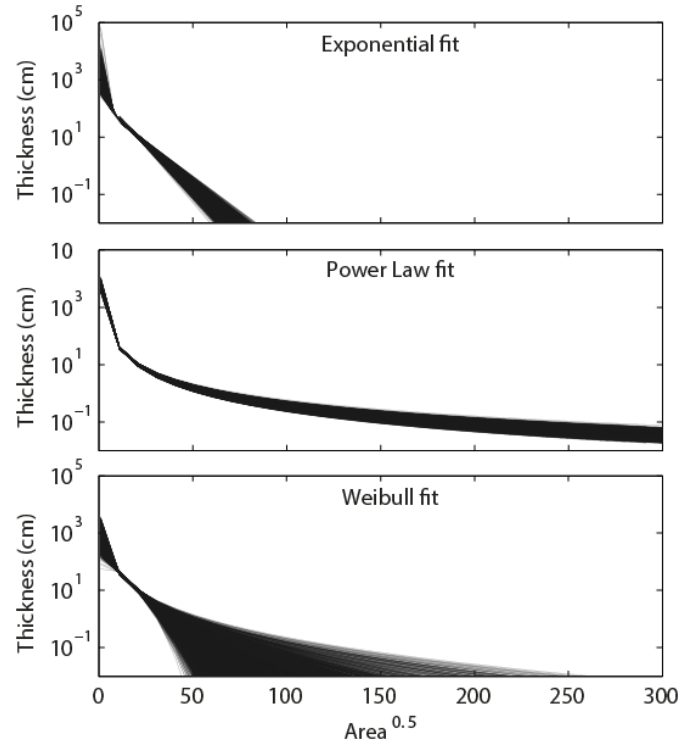
Figure 6: Compilation of the 10,000 separate fits performed during a single *Propagation* run, reflecting a variability of 10% of thickness and isopach area.

percentiles, mean and median) for each input parameter and ESP, of which Table 4 is a simplified version. Table 5 presents the median value of each ESP distribution and selected interpercentile ranges. The interpercentile ranges show the spread between pairs of percentiles expressed in percent and are defined as $|ROD_{upper} - ROD_{lower}|$. Normalized interpercentile ranges are useful for a comparison of the spreads of distributions across all ESPs.

## Discussion

The *TError* package was designed to assist researchers in characterizing the variability of ESPs for explosive eruptions. Typical field-based input parameters used to derive ESPs relate to the compilation of isopleth and isopach maps (*i.e.,* crosswind and downwind ranges of isopleth maps, diameter of maximum clasts, deposit thickness, and area of isopach contours). We do not aim to quantify the typical ranges of errors associated with field-based input parameters but strongly encourage systematic studies of the uncertainty related to the variability of deposits, measurement techniques and subjective interpretations following the works of *Barberi et al.* (1995), *Biass & Bonadonna* (2011), *Cioni et al.* (2011), *Bonadonna et al.* (2013), *Engwell et al.* (2013), *Klawonn et al.* (2014a) and *Klawonn et al.* (2014b). Four additional key input parameters are considered in the *TError* package (empirical constants of *Wilson & Walker* (1987) and *Mastin et al.* (2009), distal integration limit of *Bonadonna & Houghton* (2005) and wind speed at the tropopause) in order to assess the sensitivity related to the choice of given values. First, using the method of *Wilson & Walker* (1987), two extreme values for the constants exist, namely 0.236 and 0.295, corresponding to plume temperatures of 1,120°K and 1,300°K, respectively. In the case of Layer 5 of Cotopaxi volcano, the calculation of MER with the method of *Wilson & Walker* (1987) with a constant of 0.236 results in a MER value 140% larger than a constant of 0.295. Second,

*Mastin et al.* (2009) provide a formulation of the MER built upon the fit of well-described eruptions resulting in an empirical coefficient of 2. However, the confidence interval associated with this fit is equally as important as the central value, since a plume height of $25\,$km results in a range of MERs varying between $2 \times 10^{7}$ to $4 \times 10^{8}$ kgs$^{-1}$, with respective ROD values of $-80\%$ and $+300\%$ around the central value of about $1 \times 10^{8}$ kg s$^{-1}$. These boundary values correspond to constants of 2.9 and 1.4, respectively located at $+45\%$ and $-30\%$ around a reference value of 2. Finally, the choice of a distal limit of integration is necessary to estimate the tephra volume based on the power-law approach. *Bonadonna & Houghton* (2005) state two possible case figures based on the $m$ exponent: when $m$ is less than 2, the distal integration limit will have more impact on the final volume than when $m$ is greater than 2. For the cases of Layer 3 and Layer 5 of Cotopaxi volcano, *Biass & Bonadonna* (2011) showed how the resulting volume changed by almost $100\%$ for Layer 3 ($m = 1.76$) with distal integration limits of $100\,$km and $500\,$km, whereas the change in volume was negligible for Layer 5 ($m = 2.11$).

## Usage of the *TError* package

The purpose of *TError* is to raise awareness about the inherent uncertainty associated with the characterization of tephra deposits. We therefore encourage the user to read the thoroughly commented code and the manual and to keep a critical eye on the different outputs in order to avoid using the *TError* package as a *black box*. This is especially true for the volume calculation using the Weibull method, which is highly sensitive to initial ranges for the $\lambda$ and $n$ inputs into the optimization algorithm. By default, the code sets the ranges of $\lambda$ and $n$ based on Table 2 from, *Bonadonna & Costa* (2013), estimating VEI as a mean value between the exponential and power-law methods. In some cases, due to the wide range of shape that a Weibull distribution can adopt, the optimization used to minimize the error associated with the fit (Eq. 12) might not result in a unique solution, amongst which some might be physically impossible. The user is therefore encouraged to experiment with various ranges of $\lambda$ and $n$ values until a satisfactory and geologically realistic solution is found, namely by critically interpreting the resulting fits (Figure 5). Caveats on the use of the Weibull technique are available in *Bonadonna & Costa* (2012) and *Bonadonna & Costa* (2013).

## Propagation of error

The *TError* package uses stochastic techniques to explore the potential range of uncertainty associated with input parameters and to propagate this range through different ESPs. In the case study presented here, 10,000 runs of Monte Carlo simulations were performed where each run consists of sampling a predefined distribution for input parameters, followed by the application of the workflow shown in Figure 1, resulting in a calculation time of about 30 minutes on an Intel Xeon 2 GHz processor with 16 GB of ram. The choice of 10,000 runs of Monte-Carlo simulations was adopted following a sensitivity analysis varying the number of runs between 100 and 50,000, which showed that the median and the interpercentile ranges reached stable values after 10,000 runs.

In *TError*, a subjective choice must be made upon the initial distribution of error of input parameters. If recent studies suggest mainly lognormal distribution of errors related to measurement and deposit uncertainties (*Engwell et al.*, 2013; *Klawonn et al.*, 2014b), these systematic investigations are focused on the calculation of the erupted volume only. In *TError*, in the absence of more detailed studies on the possible shape of the uncertainty related to input parameters, we implemented Gaussian and uniform distributions of uncertainty mainly for simplicity. Both distributions, in the way they are implemented, assume that the reference value input by the user is the best possible guess and that the uncertainty will be symmetrically spread around the central value. A Gaussian distribution assumes that the error will be preferentially centered on the reference value whereas a uniform distribution assumes equal probabilities of error within the range selected by the user. The additional material comprises a comprehensive output of a propagation run assuming a uniform distribution of errors with a maximum RIU of $\pm 10\%$ and Table 5 presents the median value of all ESPs and

selected interpercentile ranges for both Gaussian and uniform distributions. These results show consistent median values for both distributions, but the spreads given by the interquartile ranges are in most cases larger for uniform random than for Gaussian distributions by about 30%. In some rare cases, the spread is larger for Gaussian than uniform random distributions (*e.g.,* volumes calculated with the method of *Fierstein & Nathenson* (1992)), which can be explained by a combination of sampling of input parameters outside the $3\sigma$ range and a sensitivity of the model to extreme values. The general nature of the resulting distributions of error (*e.g.,* symmetrical *vs.* asymmetrical) is preserved.

For this case study, wind speed was propagated from the method of *Carey & Sparks* (1986), implying a direct dependency on the crosswind range, downwind range and clast diameter. Taking the value from *Carey & Sparks* (1986) ($\approx 19\,\mathrm{m\,s^{-1}}$), the additional files comprise a tabulated output of a propagation run where the wind speed is input as an independent variable with a maximum RIU of $\pm10\%$. It can be observed that although the wind distribution resulting from the propagation of *Carey & Sparks* (1986) results in larger spreads (Q1 and Q3 at $\pm7\%$) compared to the distribution obtained by setting the wind as an independent variable (Q1 and Q3 at $\pm2\%$), the latter results in larger spreads in the ESPs dependent on the wind speed. For example, using the method of *Degruyter & Bonadonna* (2012) with wind propagated from *Carey & Sparks* (1986) Q1 and Q3 for the MER are located at $\pm5\%$ from the reference value, but are located at $\pm15\%$ when the wind is input as an independent variable. This counterintuitive result can be explained by the fact that when propagating from the method of *Carey & Sparks* (1986), individual sets of plume height and wind profiles are physically related. In contrast, sets of plume height and wind speed sampled independently tend to increase the spread because they do not reflect any physical model.

### Reporting error in ESP

The quantification of the uncertainty on ESPs with the *TError* package relies on stochastic sampling of noise around a reference value on a user-defined probability density function, with the advantage of characterizing ESPs as total distributions from which features such as asymmetry or heavy tails (*e.g.,* Figure 4f) can be observed and described (*Robert & Casella*, 2004). For this reason we favored the stochastic over the derivative approach, which tends to hide such critical aspects of error propagation. Figure 4 shows the characterization of ESPs for Layer 5 of Cotopaxi volcano, and such figures are probably the most complete way of representing the uncertainty associated with the characterization of tephra deposits. If ESPs need to be expressed as values, the asymmetry displayed by some distributions in Figure 4 suggest that *i)* the final central value must be described by the median rather than the mean, as the latter will be highly influenced by extreme values, and *ii)* the final error values must be expressed as a lower and upper bounds in order to express the asymmetry of the distribution. The choice of the percentiles used to express the uncertainty is thus critical, as the $25^{th}$-$75^{th}$, $9^{th}$-$91^{st}$ and $2^{nd}$-$98^{th}$ percentiles describe 50%, 82% and 96% of the populations, respectively. Here, we adopt the $2^{nd}$-$98^{th}$ percentiles as lower and upper boundaries, and Table 6 summarizes the ESPs for Layer 5 according to such a strategy. When several strategies are available for the quantification of a single ESP (*e.g.,* MER, volume), we chose not to average the different models in order to keep a critical control on the reported values. This is especially true for the volume calculation, for which the fits of the different strategies must be analyzed and discussed in the context of a given deposit. In the case of Layer 5, only 6 isopach contours are available, mainly representing the medial portion of the deposit, from which a proximal segment was defined on only two points. Due to this configuration, the Weibull fit is close to the exponential fit and give volumes of 0.23 and 0.29 km$^3$, respectively, whereas the power-law fit, mostly due to the lack of proximal and distal constraints, results in a volume of 0.43 km$^3$. Knowledge of the deposit suggests that the *true* value is probably located between these two extremes, and we therefore suggest reporting intervals across different strategies.

## Concluding remarks

The characterization of tephra deposits carries an inherent uncertainty, which is necessary to constrain. For this reason the *TError* package was developed. The main features of *TError* include:

- an implementation of the most frequently used strategies for the quantification of ESPs,
- the capacity to assess the sensitivity of ESPs to various field-based, empirical and model-dependent input parameters including crosswind and downwind ranges, the clast diameter, thickness measurements, area of isopach contours, empirical constants of *Wilson & Walker* (1987) and *Mastin et al.* (2009), deposit density, distal limit of the power-law integration and wind speed at the tropopause,
- the quantification of the uncertainty associated with ESPs as a function of the uncertainty of input parameters through stochastic sampling,
- the choice of two distributions of errors for input parameters, namely Gaussian and uniform random,
- the compilation of the results as a comprehensive reports and sets of figures.

The package, rather than being a shortcut to the characterization of tephra deposits, is designed to assist a systematic investigation of the impacts of uncertainty of tephra deposits on the final characterization of physical ESPs. In order to report the uncertainty associated with ESPs, we suggest using, when possible, distributions and boxplots as depicted in Figure 4. Otherwise, the median should be used with an asymmetrical confidence interval, typically the $2^{nd}$ and $98^{th}$ percentiles in order to account for 96% of the population. Applied to Layer 5 of Cotopaxi volcano, with a $\pm 10\%$ uncertainty on all input parameters, a Gaussian distribution of errors and the $2^{nd}$ and $98^{th}$ percentiles as lower and upper bounds, the results of *TError* after critical interpretation show:

- a plume height of $30 \pm 1\,\mathrm{km}$ a.s.l.,
- a maximum wind speed at the tropopause of $19 \pm 4\,\mathrm{m\,s^{-1}}$,
- a maximum MER of $1.8^{+0.3}_{-0.2} \times 10^8\,\mathrm{kg\,s^{-1}}$,
- a tephra volume between $0.23^{+0.13}_{-0.04}$ and $0.43^{+0.08}_{-0.06}\,\mathrm{km^3}$,
- an eruption duration between $24^{+12}_{-6}$ and $42^{+6}_{-12}$ minutes.

## Acknowledgments

## References

ANDRONICO, D., SCOLLO, S., CARUSO, S. & CRISTALDI, A. (2008) The 2002–03 Etna explosive activity: Tephra dispersal and features of the deposits. *Journal of Geophysical Research, Solid Earth*, **113**(B4):B04209. ISSN 2156-2202. doi:10.1029/2007JB005126. 4

BARBERI, F., COLTELLI, M., FRULLANI, A., ROSI, M. & ALMEIDA, E. (1995) Chronology and dispersal characteristics of recently (last 5000 years) erupted tephra of Cotopaxi (Ecuador): implications for long-term eruptive forecasting. *Journal of Volcanology and Geothermal Research*, **69**(3-4):217–239. 2, 8, 18

BIASS, S. & BONADONNA, C. (2011) A quantitative uncertainty assessment of eruptive parameters derived from tephra deposits: the example of two large eruptions of Cotopaxi volcano, Ecuador. *Bulletin of Volcanology*, **73**(1):73–90. 2, 8, 9, 18, 19

BONADONNA, C., BIASS, S. & COSTA, A. (accepted) Physical characterization of explosive volcanic eruptions based on tephra deposits: propagation of uncertainties and sensitivity analysis. *Journal of Volcanolology and Geothermal Research.* 3

BONADONNA, C., CIONI, R., PISTOLESI, M., CONNOR, C., SCOLLO, S., PIOLI, L. & ROSI, M. (2013) Determination of the largest clast sizes of tephra deposits for the characterization of explosive eruptions: a study of the IAVCEI commission on tephra hazard modelling. *Bulletin of Volcanology*, **75**(1):1–15. ISSN 0258-8900. doi:10.1007/s00445-012-0680-3. 2, 18

BONADONNA, C. & COSTA, A. (2012) Estimating the volume of tephra deposits: A new simple strategy. *Geology*, **40**(5):415–418. 2, 3, 5, 6, 7, 9, 10, 13, 14, 15, 16, 17, 19, 26, 27

BONADONNA, C. & COSTA, A. (2013) Plume height, volume, and classification of explosive volcanic eruptions based on the Weibull function. *Bulletin of Volcanology*, **75**(8):1–19. 2, 19

BONADONNA, C. & HOUGHTON, B. (2005) Total grain-size distribution and volume of tephra-fall deposits. *Bulletin of Volcanology*, **67**(5):441–456. 2, 3, 5, 6, 7, 9, 10, 13, 14, 15, 16, 17, 18, 19, 26, 27

BONADONNA, C. & PHILLIPS, J.C. (2003) Sedimentation from strong volcanic plumes. *Journal of Geophysical Research, Solid Earth*, **108**(B7):2340. ISSN 2156-2202. doi:10.1029/2002JB002034. 5, 7

BONASIA, R., MACEDONIO, G., COSTA, A., MELE, D. & SULPIZIO, R. (2010) Numerical inversion and analysis of tephra fallout deposits from the 472AD sub-Plinian eruption at Vesuvius (Italy) through a new best-fit procedure. *Journal of Volcanology and Geothermal Research*, **189**(3-4):238–246. doi:10.1016/j.jvolgeores.2009.11.009. URL http://www.sciencedirect.com/science/article/pii/S0377027309004417. 3

BURDEN, R., PHILLIPS, J. & HINCKS, T. (2011) Estimating volcanic plume heights from depositional clast size. *Journal of Geophysical Research, Solid Earth*, **116**(B11):B11206. 2

BURDEN, R.E., CHEN, L. & PHILLIPS, J.C. (2013) A statistical method for determining the volume of volcanic fall deposits. *Bulletin of Volcanology*, **75**(6):1–10. ISSN 0258-8900. doi:10.1007/s00445-013-0707-4. URL http://dx.doi.org/10.1007/s00445-013-0707-4. 2, 3

CAREY, S. & SPARKS, R. (1986) Quantitative models of the fallout and dispersal of tephra from volcanic eruption columns. *Bulletin of Volcanology*, **48**(2-3):109–125. 2, 3, 4, 7, 9, 10, 13, 14, 15, 16, 17, 20, 26, 27

CIONI, R., BERTAGNINI, A., ANDRONICO, D., COLE, P.D. & MUNDULA, F. (2011) The 512 AD eruption of Vesuvius: complex dynamics of a small scale subplinian event. *Bulletin of Volcanology*, **73**(7):789–810. ISSN 0258-8900. doi:10.1007/s00445-011-0454-3. 2, 18

CONNOR, L.J. & CONNOR, C.B. (2006) Inversion is the key to dispersion: understanding eruption dynamics by inverting tephra fallout. *In* H.M. MADER, S.G. COLES, C.B. CONNOR & L.J. CONNOR (eds.) *Statistics in Volcanology*, number 1 in Special Publications for IAVCEI, 231–242. Geological Society of London, London. 3

DAGGITT, M.L., MATHER, T.A., PYLE, D.M. & PAGE, S. (2014) AshCalc – a new tool for the comparison of the exponential, power-law and Weibull models of tephra deposition. *Journal of Applied Volcanology*, **3**(1):7. ISSN 2191-5040. doi:10.1186/2191-5040-3-7. 5, 6

DEGRUYTER, W. & BONADONNA, C. (2012) Improving on mass flow rate estimates of volcanic eruptions. *Geophysical Research Letters*, **39**(16). doi:10.1029/2012GL052566. 2, 3, 5, 7, 9, 10, 13, 14, 15, 16, 17, 20

ENGWELL, S.L., SPARKS, R.S.J. & ASPINALL, W.P. (2013) Quantifying uncertainties in the measurement of tephra fall thickness. *Journal of Applied Volcanology*, **2**(1):1–12. doi:10.1186/2191-5040-2-5. URL http://dx.doi.org/10.1186/2191-5040-2-5. 2, 18, 19

FIERSTEIN, J. & NATHENSON, M. (1992) Another look at the calculation of fallout tephra volumes. *Bulletin of Volcanology*, **54**(2):156–167. 2, 3, 5, 7, 9, 10, 13, 14, 15, 16, 17, 20, 25, 27

GONZÁLEZ-MELLADO, A. & CRUZ-REYNA, S. (2010) A simple semi-empirical approach to model thickness of ash-deposits for different eruption scenarios. *Natural Hazards, Earth System Science*, **10**(11):2241–2257. 5

KLAWONN, M., HOUGHTON, B., SWANSON, D., FAGENTS, S., WESSEL, P. & WOLFE, C. (2014*a*) Constraining explosive volcanism: subjective choices during estimates of eruption magnitude. *Bulletin of Volcanology*, **76**(2):1–6. ISSN 0258-8900. doi:10.1007/s00445-013-0793-3. URL http://dx.doi.org/10.1007/s00445-013-0793-3. 2, 18

KLAWONN, M., HOUGHTON, B., SWANSON, D., FAGENTS, S., WESSEL, P. & WOLFE, C. (2014*b*) From field data to volumes: constraining uncertainties in pyroclastic eruption parameters. *Bulletin of Volcanology*, **76**(7):1–16. ISSN 0258-8900. doi:10.1007/s00445-014-0839-1. URL http://dx.doi.org/10.1007/s00445-014-0839-1. 18, 19

KLAWONN, M., WOLFE, C.J., FRAZER, L.N. & HOUGHTON, B.F. (2012) Novel inversion approach to constrain plume sedimentation from tephra deposit data: Application to the 17 June 1996 eruption of Ruapehu volcano, New Zealand. *Journal of Geophysical Research, Solid Earth*, **117**(B5):B05205. ISSN 2156-2202. doi:10.1029/2011JB008767. 3

LEGROS, F. (2000) Minimum volume of a tephra fallout deposit estimated from a single isopach. *Journal of Volcanology and Geothermal Research*, **96**(1-2):25–32. 2

MASTIN, L., GUFFANTI, M., SERVRANCKX, R., WEBLEY, P., BARSOTTI, S., DEAN, K., DURANT, A., EWERT, J., NERI, A., ROSE, W.I., SCHNEIDER, D., SIEBERT, L., STUNDER, B., SWANSON, G., TUPPER, A., VOLENTIK, A. & WAYTHOMAS, C. (2009) A multidisciplinary effort to assign realistic source parameters to models of volcanic ash–cloud transport and dispersion during eruptions. *Journal of Volcanology and Geothermal Research*, **186**(1–2):10–21. 2, 3, 4, 6, 7, 9, 10, 13, 14, 15, 16, 17, 18, 19, 21, 26, 27

MORTON, B.R., TAYLOR, G. & TURNER, J.S. (1956) Turbulent Gravitational Convection from Maintained and Instantaneous Sources. *Proceedings of the Royal Society, London, Series A. Mathematical and Physical Sciences*, **234**(1196):1–23. doi:10.1098/rspa.1956.0011. 4

ODDSSON, B., GUDMUNDSSON, M., LARSEN, G. & KARLSDÓTTIR, S. (2012) Monitoring of the plume from the basaltic phreatomagmatic 2004 Grímsvötn eruption – application of weather radar and comparison with plume models. *Bulletin of Volcanology*, **74**(6):1395–1407. doi:10.1007/s00445-012-0598-9. 2

PREJEAN, S.G. & BRODSKY, E.E. (2011) Volcanic plume height measured by seismic waves based on a mechanical model. *Journal of Geophysical Research, Solid Earth*, **116**(B1):B01306. ISSN 2156-2202. doi:10.1029/2010JB007620. 2

PYLE, D. (1989) The thickness, volume and grainsize of tephra fall deposits. *Bulletin of Volcanology*, **51**(1):1–15. 2, 5

RIPEPE, M., BONADONNA, C., FOLCH, A., DELLE DONNE, D., LACANNA, G., MARCHETTI, E. & HÖSKULDSSON, A. (2013) Ash-plume dynamics and eruption source parameters by infrasound and thermal imagery: The 2010 Eyjafjallajökull eruption. *Earth and Planetary Science Letters*, **366**:112–121. doi: 10.1016/j.epsl.2013.02.005. 2

ROBERT, C.P. & CASELLA, G. (2004) *Monte Carlo Statistical Methods*, volume 96. Springer, New York, 2$^{nd}$ edition. ISBN 0387212396. 3, 20

SCOLLO, S., DEL CARLO, P. & COLTELLI, M. (2007) Tephra fallout of 2001 Etna flank eruption: Analysis of the deposit and plume dispersion. *Journal Volcanology and Geothermal Research*, **160**(1-2):147–164. ISSN 03770273. doi:10.1016/j.jvolgeores.2006.09.007. URL http://www.sciencedirect.com/science/article/pii/S0377027306003544. 4

SPARKS, R. (1986) The dimensions and dynamics of volcanic eruption columns. *Bulletin of Volcanology*, **48**(1):3–15. 2

SPARKS, R.S.J., BURSIK, M.I., CAREY, S.N., GILBERT, J., GLAZE, L.S., SIGURDSSON, H. & WOODS, A.W. (1997) *Volcanic Plumes*. Wiley. ISBN 0471939013. 2

THORARINSSON, S. (1954) The eruption of Hekla, 1947-48, 3, The tephra-fall from Hekla, March 29th, 1947. *Visindafélag Íslendinga*, **2**:1–68. 2

THORARINSSON, S. (1967) The eruption of Hekla 1947-1948: I. the eruptions of Hekla in historical times. A tephrochronological study. *Soc Scientiarum Islandica*, 1–199. 2

VOLENTIK, A.C.M., CONNOR, C.B., CONNOR, L.J. & BONADONNA, C. (2009) Aspects of volcanic hazards assessment for the Bataan nuclear power plant, Luzon Peninsula, Philippines. *In* C. CONNOR, N.A. CHAPMAN & L. CONNOR (eds.) *Volcanic and Tectonic Hazard Assessment for Nuclear Facilities*, 229 – 256. Cambridge University Press, Cambridge. 3

WEHRMANN, H., BONADONNA, C., FREUNDT, A. & HOUGHTON, B. (2006) Fontana Tephra: A basaltic Plinian eruption in Nicaragua. *In* W.I. ROSE, G.J.S. BLUTH, M.J. CARR, J.W. EWERT, L.C. PATINO & J.W. VALLANCE (eds.) *Volcanic Hazards in Central America*, volume 412 of *Geological Society of America, Special Papers*, 209–224. 4

WILSON, L. & WALKER, G. (1987) Explosive volcanic eruptions - VI. Ejecta dispersal in plinian eruptions: the control of eruption conditions and atmospheric properties. *Geophysical Journal of the Royal Astronomical Society*, **89**(2):657–679. 2, 3, 4, 7, 9, 10, 13, 14, 15, 16, 17, 18, 21, 26, 27

WOODHOUSE, M.J., HOGG, A.J., PHILLIPS, J.C. & SPARKS, R.S.J. (2013) Interaction between volcanic plumes and wind during the 2010 Eyjafjallajökull eruption, Iceland. *Journal of Geophysical Research, Solid Earth*, **118**(1):92–109. ISSN 2169-9356. doi:10.1029/2012JB009592. 2

# Additional files

The following additional files are available for download:

- Matlab source code and user manual of the *TError* package (`TError_code.zip`),
- complete output of a sensitivity run for Layer 5 of Cotopaxi volcano (`Coto_L5_sensitivity.xlsx`),
- complete output of a propagation run for Layer 5 of Cotopaxi volcano using a Gaussian distribution of error (`Coto_L5_Gaussian_propagation.xlsx`),
- complete output of a propagation run for Layer 5 of Cotopaxi volcano using a Gaussian distribution of error and a wind speed input as an independent variable (`Coto_L5_Gaussian_propagation_wind.xlsx`),
- complete output of a propagation run for Layer 5 of Cotopaxi volcano using a uniform distribution of error (`Coto_L5_Uniform_propagation.xlsx`).

The compressed archive (`TError_code.zip`) contains *(i)* a user manual (`TError.pdf`), *(ii)* two Matlab scripts `TError_sensitivity.m`, necessary for running the *TError* sensitivity analysis, and `TError_propagation.m`, necessary for running the *TError* error propagation analysis, and *(iii)* two additional folders within the main (*root*) folder, `dep`, containing Matlab macros (source codes that the two main scripts depend on), and `Output`, where all result files are stored after processing.

# How to run the macros

1. Copy, rename and edit the example file, `isopach_example.txt`. This file should contain isopach data (*i.e.,* area of isopach contours in km$^2$ *vs.* deposit thickness in cm). Note that the first row indicates the location of the breaks in slope for the exponential method of *Fierstein & Nathenson* (1992). Refer to the *TError* user manual for a precise description of the file format.
2. Edit lines $22 - 80$ of the `TError_sensitivity.m` file.
3. Edit the lines $22 - 94$ of the `TError_propagation.m` file.
4. Run each of scripts by typing their name in the Matlab command window.

# Code descriptions

*TError* requires user input related to the compilation of isopleth and isopach maps and for the different models used for the characterization of ESPs. Before running the code, it is necessary to define an error distribution that will be applied to all variable parameters. With the *TError* package, both Gaussian and uniform random distributions are implemented. For each variable parameter, define a relative error in percent. If a Gaussian error distribution is chosen, the error will represent the $3\sigma$ of the distribution. If a uniform random distribution is chosen, the error will represent the lower and upper bounds. *TError* input parameters are defined below.

**General**

| | |
|---|---|
| `run_nm` | Run name |
| `vent_ht` | Vent height (m a.s.l.) |
| `trop_ht` | Tropopause height (m a.s.l.) |
| `nb_sims` | Number of Monte Carlo simulations |
| `error_d` | Error distribution (1. Uniform or 2. Gaussian) |
| `rangeE` | Error vector for the sensitivity analysis, entered as: $error_{min} : interval : error_{max}$ |

**Plume Height and Wind Speed**

cl_d   Clast density used for the compilation of isopleth maps, invariable in *TError*

dm_v   Maximum clast diameter in cm for the isopleth contours in *Carey & Sparks* (1986)

dm_e   Error on clast diameter in %

dw_v   Downwind range in km as defined in *Carey & Sparks* (1986)

dw_e   Error on downwind range in %

cw_e   Crosswind range in km as defined in *Carey & Sparks* (1986)

cw_e   Error on crosswind range in %

**Mass Eruption Rate (MER)**

cstWW_v   Constant as defined in *Wilson & Walker* (1987)

cstWW_e   Error on constant in %

cstMa_v   Constant as defined in *Mastin et al.* (2009)

cstMa_e   Error on constant in %

wind_v   Maximum wind speed at the tropopause in $m\,s^{-1}$; use a value of $-1$ to propagate the wind from *Carey & Sparks* (1986)

wind_e   Error on maximum wind speed in %

**Volume**

fl   File containing isopach data (described later); should be located in the root folder of the *TError* package; *e.g.,* see file isopach_example.txt

C_v   Distal integration limit in km for the method of *Bonadonna & Houghton* (2005)

C_e   Error on distal integration limit in %

lam_r   Initial range of $\lambda$ for the method of *Bonadonna & Costa* (2012), entered as: $\lambda_{min}, \lambda_{max}$

n_r   Initial range of $n$ for the method of *Bonadonna & Costa* (2012), entered as: $n_{min}, n_{max}$

**Mass**

dep_d_v   Bulk deposit density in $kg\,m^{-3}$

dep_d_e   Error on bulk deposit density in %

**Plots and Reports**

plt   Use 1 to produce plots, else use 0

frmt   Format for saving the plots, *e.g.,* .eps, .png

max_err   Maximum range of error to plot

pcile   Percentiles to be included in the report. Pairs of percentiles should be symmetrical

# Function files

The *TError* package contains the following Matlab functions; all are located in the dep folder. These functions are executed by the main *TError* scripts based on values assigned to the input parameters described previously.

| | |
|---|---|
| `bc2012.m` | Matlab macro for calculating a Weibull fit |
| `bh2005.m` | Matlab macro for calculating a power-law fit |
| `fminsearchbnd.m` | Optimization script for the Weibull fit written by John D'Errico File Exchange 8277 |
| `fn1992.m` | Matlab macro for calculating an exponential fit |
| `get_height_CS86.m` | Matlab macro for calculating plume height and wind speed as defined in *Carey & Sparks* (1986) |
| `get_MER_DB12.m` | MER calculation using the method of *Bonadonna & Costa* (2012) |
| `get_MER_M09.m` | MER calculation using the method of *Mastin et al.* (2009) |
| `get_MER_WW87.m` | MER calculation using the method of *Wilson & Walker* (1987) |
| `get_vol_BC12.m` | Volume calculation using the method of *Bonadonna & Costa* (2012) |
| `get_vol_BH05.m` | Volume calculation using the method of *Bonadonna & Houghton* (2005) |
| `get_vol_FN92.m` | Volume calculation using the method of *Fierstein & Nathenson* (1992) |
| `get_WBL_ranges.m` | Matlab macro for setting ranges for $\lambda$ and $n$ for the Weibull optimization algorithm |
| `linspecer.m` | Readable color map written by Jonathan Lansey File Exchange 42673 |
| `nhist.m:` | Matlab function for plotting the TError_propagation results. Written by Jonathan Lansey File Exchange 27388 |
| `plot_fits_seps.m` | Generate volume fit plots performed during the Monte Carlo simulations separately |
| `plot_fits.m` | Generate fit plots for reference values of thickness measurements and areas of isopach contours |
| `plot_results.m` | Main function for plotting the results of the TError_propagation code |
| `prctile.m` | Matlab macro that returns the selected percentile |
| `rand_err` | Matlab macro that returns relative and absolute error vectors |
| `writefile.m` | Matlab macro to write the TError_propagation report |

**Disclaimer:**  The journal and author make no assertions that these program macros are without errors. Users do so at their own risk. The macros may be used without payment or permission provided the source paper is cited.